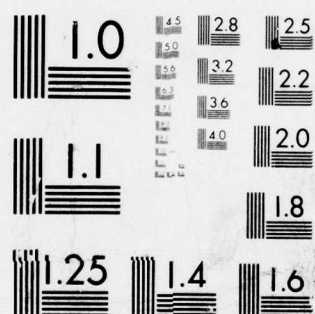AD-A075 706   AEROSPACE CORP EL SEGUNDO CA ENGINEERING GROUP   F/G 3/1
              DIGITAL SIMULATION OF A MULTISPECTRAL SCANNING SENSOR SYSTEM.(U)
              OCT 78   R G NISHINAGA , K K WONG   F04701-78-C-0079
UNCLASSIFIED TR-0079(4901-03)-4   SAMSO-TR-79-59   NL

AD
A075706

END
DATE
FILMED
12-79
DDC

MICROCOPY RESOLUTION TEST CHART
NATIONAL BUREAU OF STANDARDS-1963-A

(12) **LEVEL** II

Digital Simulation of a Multispectral Scanning Sensor System

R. G. NISHINAGA and K. K. WONG
Guidance and Control Division
Engineering Group
The Aerospace Corporation
El Segundo, Calif. 90245

1 Oct 1978

DDC

RECEIVED
OCT 30 1979

B

Final Report

79 10 29 130

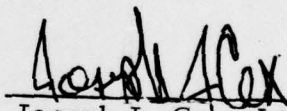This final report was submitted by The Aerospace Corporation, El Segundo, CA 90245, under Contract No. F04701-78-C-0079 with the Space and Missile Systems Organization (AFSC), Los Angeles, CA 90009. It was reviewed and approved for The Aerospace Corporation by D. J. Griep, Engineering Group. Lieutenant James C. Garcia, DYXT, was the Deputy for Technology project engineer.
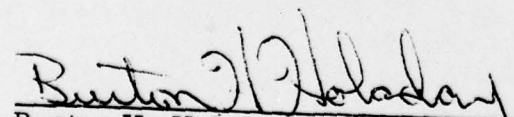
This report has been reviewed by the Information Office (OI) and is releasable to the National Technical Information Service (NTIS). At NTIS, it will be available to the general public, including foreign nationals.

This technical report has been reviewed and is approved for publication.

James C. Garcia, Lieutenant, USAF
Project Engineer

Joseph J. Cox, Lt. Col., USAF
Chief, Advanced Technology
Division

FOR THE COMMANDER

Burton H. Holaday, Colonel, USAF
Director of Technology, Plans
and Analysis

REPORT DOCUMENTATION PAGE		READ INSTRUCTIONS BEFORE COMPLETING FORM
1. REPORT NUMBER SAMSO-TR-79-59	2. GOVT ACCESSION NO.	3. RECIPIENT'S CATALOG NUMBER
4. TITLE (and Subtitle) DIGITAL SIMULATION OF A MULTISPECTRAL SCANNING SENSOR SYSTEM.		5. TYPE OF REPORT & PERIOD COVERED Final reptis
		6. PERFORMING ORG. REPORT NUMBER TR-0079(4901-03)-4
7. AUTHOR(s) R. G. Nishinaga K. K. Wong		8. CONTRACT OR GRANT NUMBER(s) F04701-78-C-0079
9. PERFORMING ORGANIZATION NAME AND ADDRESS The Aerospace Corporation El Segundo, Calif. 90245		10. PROGRAM ELEMENT, PROJECT, TASK AREA & WORK UNIT NUMBERS
11. CONTROLLING OFFICE NAME AND ADDRESS Space & Missile Systems Organization, AFSC Los Angeles Air Force Station, P.O. Box 92960 Worldway Postal Center, Los Angeles, Calif.		12. REPORT DATE 1 Oct 978
		13. NUMBER OF PAGES 24
14. MONITORING AGENCY NAME & ADDRESS(if different from Controlling Office)		15. SECURITY CLASS. (of this report) Unclassified
		15a. DECLASSIFICATION/DOWNGRADING SCHEDULE

16. DISTRIBUTION STATEMENT (of this Report)

Approved for public release; distribution unlimited

17. DISTRIBUTION STATEMENT (of the abstract entered in Block 20, if different from Report)

18. SUPPLEMENTARY NOTES

19. KEY WORDS (Continue on reverse side if necessary and identify by block number)

Simulation Models and Techniques

Sensors, Astronomical

20. ABSTRACT (Continue on reverse side if necessary and identify by block number)

This report presents a fast, efficient method for simulating multispectral scanning astronomical sensors. A general description of different simulation approaches is discussed. The models used in the proposed method to characterize the sensor and its major radiation sources are presented. These models are developed to describe the basic signals and noise in the system. The structure and features of the resulting simulation are discussed. Representative sample outputs of the simulation are presented.

DD FORM 1473
(FACSIMILE)

411 279

CONTENTS

FIGURES

INTRODUCTION

There is a growing realization that computer simulations are valuable tools for investigating the characteristics and performance of complex sensor systems. In fact, many simulations are used to evaluate proposed sensor designs and to assess processing schemes associated with the sensed data. The effectiveness of such simulations depends on the accuracy of the simulation models used to represent the actual scene, the sensor components and the associated processing. Furthermore, the techniques used to implement these models affect the efficiency and costs associated with running the simulation.

These considerations are especially significant in the simulation of future space-based scanning sensors providing deep space astronomical measurements[1,2]. These sensors are expected to scan the celestial sky and detect a number of objects (e.g., stars, resident space objects, zodiacal light). The simulation is required to simulate the sensor detection process with high fidelity and computational speed. These conditions are difficult to satisfy because the simulation must accommodate high density star fields present near the galactic equator. In general, high star density not only increases the amount of memory required by the computer simulation but also reduces the speed at which simulation must operate to achieve reasonable accuracy.

This paper presents a method for simulating a multi-spectral scanning sensor in a fast, efficient manner. The models and techniques used to accommodate the major radiation sources are discussed. Then the specific structure and capabilities of the simulation are presented. The computational requirements are assessed, and representative sample outputs of the simulation are presented. The final section is devoted to conclusions.

SYSTEM DESCRIPTION

The system to be simulated is a spaced-based, multi-spectral scanning sensor designed to collect information on celestial objects and events. As shown in Figure 1, the major on-board components of a typical system include an optics and scanner subsystem, an array of detector cells, a set of amplifiers and filters, and a multiplexer and encoder. Optical elements scan the celestial sky and focus incoming radiation onto the array of detectors located at the focal plane. Sensitive to a specific spectral region, the detector array converts the radiation through the amplifiers to voltage levels. In turn, these amplifier outputs are filtered, multiplexed and encoded for transmission to the ground.
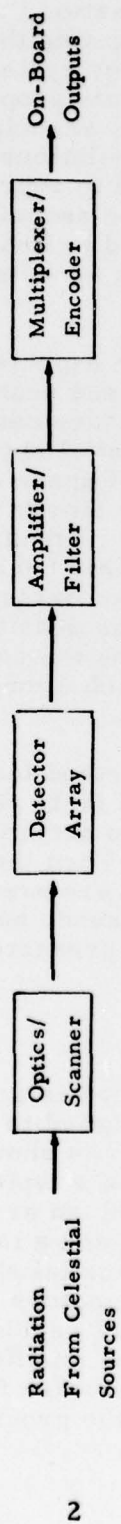
Radiation From Celestial Sources → Optics/Scanner → Detector Array → Amplifier/Filter → Multiplexer/Encoder → On-Board Outputs

Figure 1. Block Diagrams of a Scanning Sensor System

2

Sources of radiation affecting the sensor outputs include point sources such as stars and resident space objects, as well as extended sources such as zodiacal light and earth limb radiation. In addition, there are impulsive sources due to the incidence of nuclear particles and/or radiation on the detectors. All of these effects should be accommodated by the simulation.

SIMULATION TECHNIQUES

In general, a simulation of this system requires a description of the spectral, spatial and temporal characteristics of the scene and the sensor. This is exemplified by the power incident on a rectangular detector by a radiation source, which can be expressed as

$$P_{ij}(t) = \int_{-\infty}^{\infty} d\lambda \iint_{A_{Dj}} dx\, dy \iint_{-\infty}^{\infty} H_i(u, v, \lambda)\, G(u-x, v-y, \lambda) du\, dv \quad (1)$$

where $P_{ij}(t)$ denotes the power on detector j by source i at time t, H_i denotes the spectral irradiance at the image plane due to source i, G represents the optical point spread function, and A_{Dj} represents the area of detector j. The terms x, y and u, v denote the dependent variables representing space coordinates; λ denotes the spectral wavelength. Time is implicitly related to the space coordinates by the motion of the scanner. The above integrals can be interchanged to appear as

$$P_{ij}(t) = \int_{-\infty}^{\infty} d\lambda \iint_{-\infty}^{\infty} H_i(u, v, \lambda)\, du\, dv \iint_{A_{Dj}} G(u-x, v-y, \lambda) dx\, dy \quad (2)$$

The above power expressions can be solved indirectly by a Fourier transform method[3]. This method involves solving the convolution integral of (1) in the transformed spatial frequency domain, relating the temporal frequency to the spatial frequency by the scanning rate, and then inverting the resulting transform to the time doman. To obtain the transformed signal at the filter output, the frequency transform of the detector, amplifier, and filter is multiplied by the transform of $P_{ij}(t)$, prior to the inversion process (assuming linear models for these components). Then the time domain signal is obtained by inversion. To simulate the effects of noise from background sources (e.g., zodiacal light) and onboard sources, the power spectral density (PSD) of these sources is computed off-line based on the input PSD and the system transfer function. Then a random number generator is used to simulate noise corresponding to the second-order statistics of the resulting PSD. The availability of Fast

3

Fourier Transform packages provides an economic means to implement this method[4]. However, to simulate a large array with high resolution detectors, the amount of computation required to achieve the desired accuracy may become prohibitive.

A more direct approach for implementing the above relations is to make reasonable approximations and solve the convolution integral directly in the space domain. Depending on the amount of approximation, two basic methods can be identified: a "brute-force" numerical method, and a semi-analytical method. Referring to (2), the numerical method first evaluates the integrals involving the point spread function G for a given detector geometry during simulation initialization. This defines a weighting function at every point in a two-dimensional grid. At each time instant t, the weighting function is multiplied by the irradiance H_i and the result is integrated to obtain $P_{ij}(t)$ via a double summation over an area about detector j. The final integration over wavelength λ is avoided by utilizing the average of H_i and G over a spectral bandwidth $\Delta\lambda$. When the radiation is a point source, the method reduces to a simple multiplication of its intensity by the weighting function to obtain the power $P_{ij}(t)$.[5]

The potential problem with this numerical method is that a small grid spacing may be required to achieve the desired fidelity, especially for simulating extended sources. As a rule, the grid spacing will be some fraction of the smallest detail of interest (e.g., the detector dimensions, star separation distance, optical blur size). If the required number of grid points becomes large, the simulation may be too slow or expensive to run.

The semi-analytical method avoids the above problem by making simplifying assumptions on the radiation source, optical properties and/or array geometry. These assumptions permit the integrals in (1) or (2) to be evaluated analytically. As a result, the incident power is expressed in terms of known functions which can be efficiently implemented in a simulation.

SIMULATION ASSUMPTIONS

The simulation under consideration uses the semi-analytical approach to characterize the signal and noise of the scanning system. The assumptions used to simplify the sensor are given as follows:

4

1. Gaussian point spread function

$$G(x, y, \lambda) = \frac{D_o(\lambda)}{2\pi \sigma_b^2} \exp\left[\frac{-(x^2 + y^2)}{2\sigma_b^2}\right] \tag{3}$$

where σ_b denotes the optical blur size and D_o represents the spectral transmission function of the optics.

2. Bandpass optical filter

$$D_o(\lambda) = \begin{cases} 1, & \lambda_n - \frac{\Delta\lambda}{2} \leq \lambda \leq \lambda_n + \frac{\Delta\lambda}{2} \\ 0, & \text{otherwise} \end{cases} \tag{4}$$

where λ_n and $\Delta\lambda$ denote the nominal frequency and bandwidth, respectively.

3. Rectangular aperture function

$$D_{Aj}(x, y) = \begin{cases} 1, & |x-x_{cj}| \leq w/2, \quad |y-y_{cj}| \leq \ell/2 \\ 0, & \text{otherwise} \end{cases} \tag{5}$$

where w and ℓ denote the detector width and length, respectively; x_{cj} and y_{cj} define the center location of detector j in the image plane.

4. Constant nominal scan rate

$$x_{cj}(t) = x_{cj}(t_o) + v_s t + p_x(t) \tag{6}$$

$$y_{cj}(t) = y_{cj}(t_o) + p_y(t) \tag{7}$$

where v_s denotes the scan rate; p_x and p_y define small variations in the detector's position due to spacecraft attitude motion or scanning jitter; and t_o denotes the initial reference time.

5

5.   Linear Detector/Amplifier Response

$$\dot{z}_j = -\frac{1}{\tau_a} z_j + \frac{R_a}{\tau_a} (u_j + n_{Ej} + n_{Ij}) \tag{8}$$

where z_j denotes the amplifier output of detector j; R_a and τ_a represent the amplifier gain and time constant, respectively; u_j denotes the total signal incident on detector j due to point sources; n_{Ej} and n_{Ij} represent noise on detector j due to extended sources and impulsive sources, respectively.

6.   Linear Filter Response

$$\dot{q}_j = Aq_j + bz_j \tag{9}$$

where q_j denotes an $n \times 1$ state vector of the on-board filter; A and b represent $m \times n$ and $n \times 1$ matrices, respectively.

SIGNAL AND NOISE RELATIONS

Sources of radiation are modeled in the simulation as point sources, extended sources, or impulsive sources. Point sources which include stars and resident space objects produce the basic signals of the system. Extended sources such as zodiacal light and impulsive sources such as high energy nuclear particles are assumed to produce noise at the detector.

The spectral irradiance of point sources can be expressed at the image plane as

$$H_i(u, v, \lambda) = \eta_o A_o H_{Ni}(\lambda) \, \delta(u - u_{oi}) \, \delta(v - v_{oi}) \tag{10}$$

where

$$H_{Ni}(\lambda) = \begin{cases} H_{Si}(\lambda), & \text{Star} \\[2ex] \dfrac{J_{Ti}(\lambda)}{R^2}, & \text{Resident Space Object} \end{cases} \tag{11}$$

The terms η_o and A_o respectively denote the optical efficiency and optical entrance area; H_{Si} is the irradiance of star source i; J_{Ti} and R represent the intensity and range of resident space object i, respectively; $\delta(\bullet)$ denotes the Dirac Delta function; and u_{oi} and v_{oi} define the location of the point sources in the image plane.

6

Combining Eqs. (3) through (7) into (1) yields the incident power on detector j due to point source i as

$$P_{ij}(t) = \frac{1}{4} \eta_o A_o \Delta\lambda \, H_{Ni}(\lambda_n) \, Z(x_{cj} - u_{oi}, w) \, Z(y_{cj} - v_{oi}, \ell) \quad (12)$$

where

$$Z(u-v, a) = erf\left(\frac{u-v + a/2}{\sqrt{2}\sigma_b}\right) - erf\left(\frac{u-v - a/2}{\sqrt{2}\sigma_b}\right) \quad (13)$$

$$erf(x) = \frac{2}{\sqrt{\pi}} \int_o^x \exp(-\xi^2) \, d\xi \quad (14)$$

The signal u_j to the amplifier includes all incident power on detector j due to point sources, or

$$u_j = \sum_{i=1}^{N_{Pj}} P_{ij}(t) \quad (15)$$

where N_{Pj} represents the total number of point sources affecting detector j.

Extended radiation sources are assumed to produce random photon noise at the detector. To a first order approximation, the statistics of photon noise depend on the incident power resulting from these sources. A measure of this power can be estimated by assuming that the radiance due to these sources is primarily unstructured in the scanned region. In this case the irradiance H_i from extended source i at the image plane can be expressed as

$$H_i(x, y, \lambda) = \frac{\eta_o A_o}{f^2} N_{Bi}(\lambda) \quad (16)$$

where f denotes the focal length of the optics; N_{Bi} represents the unstructured component of the radiance from source i. Substituting (16), (3), and (4) into (1) yields the power on detector j due to the extended source i as

$$P_{ij} = \frac{\eta_o A_o}{f^2} N_{Bi}(\lambda_n) A_{Dj} \Delta\lambda \quad (17)$$

7

In this case, the resulting photon noise n_{Ej} at detector j is modeled as a white Gaussian random variable with mean $\bar{n}_E$ and auto-correlation function $R_E(\tau)$ given as follows:

$$\bar{n}_E = \sum_{i=1}^{N_{Ej}} P_{ij} \tag{18}$$

$$R_E(\tau) = Q_E \, \delta(t-\tau) \tag{19}$$

where

$$Q_E = \frac{2 \, E_n \left[\sum_{i=1}^{N_{Ej}} P_{ij} + \sum_{i=1}^{N_{Pj}} P_{ij} \right]}{\eta_Q} \tag{20}$$

The term E_n represents the energy of a photon at wavelength λ_n; η_Q is the quantum efficiency; and N_{Ej} is the total number of extended sources affecting detector j.

Impulsive sources are modeled as an impulse noise process at the detector[6]. In the time interval $(0, T)$, the process consists of N_{Ij} independent pulses on detector j with a common waveform, the ith pulse having an amplitude a_{ij} and time of occurence τ_{ij}. Thus, the impulse noise n_{Ij} can be expressed as

$$n_{Ij} = \sum_{i=1}^{N_{Ij}} a_{ij} u(t - \tau_{ij}) \quad , \quad 0 \leq t \leq T \tag{21}$$

where u represents the pulse waveform.

It is assumed that the amplitudes a_{ij} are statistically independent random variables, characterized by a known density function f_a. Also, the arrival times τ_{ij} are assumed to be uniformly and independently distributed in $(0, T)$. As a result, the number of pulses arriving in a given time interval $(0, T)$ follows a Poisson distribution characterized by a mean rate of arrival λ_I.[7] The waveform u can be modeled by the Dirac Delta function at the amplifier input. Thus, given f_a, λ_I, and u, the impulse noise process is specified.

8

To describe the signals and noise for a computer simulation, a set of difference equations is developed. Under the above assumptions, Eq. (8) of the amplifier can be integrated between times t_n and t_{n+1} to yield

$$z_j(t_{n+1}) = e^{-\Delta/\tau_a} z_j(t_n) + w_{Uj}(t_{n+1}) + w_{Ej}(t_{n+1}) + w_{Ij}(t_{n+1}) \quad (22)$$

where

$$w_{Uj}(t_{n+1}) = \frac{R_a}{\tau_a} \int_{t_n}^{t_n+\Delta} e^{-(t_n+\Delta-\tau)/\tau_a} u_j(\tau)d\tau \quad (23)$$

$$w_{Ij}(t_{n+1}) = \frac{R_a}{\tau_a} \sum_{i=1}^{N_{Ij}} a_{ij} e^{-(t_n+\Delta-\tau_{ij})/\tau_a} \quad , \quad t_{n+1} \geq \tau_{ij} \quad (24)$$

where Δ represents the integration time $(t_{n+1}-t_n)$. The term w_{Ej} is a white Gaussian random noise sequence with mean $\overline{w}_E$ and variance σ_E^2 specified as

$$\overline{w}_E = R_a \overline{n}_E \quad (25)$$

$$\sigma_E^2 = R_a^2 Q_E \left[1 - e^{-2\Delta/\tau_a} \right] /2\tau_a \quad (26)$$

In a similar manner, the difference equation for the filter can be expressed as

$$q_j(t_{n+1}) = e^{A\Delta} q_j(t_n) + v_j(t_{n+1}) \quad (27)$$

where

$$v_j(t_{n+1}) = \int_{t_n}^{t_n+\Delta} e^{A(t_n+\Delta-\tau)} bz_j(\tau)d\tau \quad (28)$$

The integrals of (23) and (28) can be evaluated by making an approximation on the forcing term such as

$$u_j(t_{n+1} - \tau) \cong u_j(t_{n+1}) - \dot{u}_j(t_{n+1})\tau \qquad (29)$$

$$z_j(t_{n+1} - \tau) \cong z_j(t_{n+1}) - \dot{z}_j(t_{n+1})\tau \qquad (30)$$

where

$$\dot{u}_j(t_{n+1}) = \frac{1}{\Delta}\left[u_j(t_{n+1}) - u_j(t_n)\right] \qquad (31)$$

$$\dot{z}_j(t_{n+1}) = \frac{1}{\Delta}\left[z_j(t_{n+1}) - z_j(t_n)\right] \qquad (32)$$

Substituting the above relations into (23) and (28) yields expressions for w_{Uj} and v_j, respectively, which are explicitly related to u_j and z_j at times t_{n+1} and t_n. These difference relations are readily incorporated in a digital computer simulation.

Because of the closed-form solution to the amplifier and filter equations, the integration step size is not limited by the minimum time constant of the system. Instead, the step size is selected to provide sufficient accuracy in the approximation of (29) - (32). Reasonable accuracy can be achieved by allowing a sufficient number of integration steps within the detector's dwell time (w/v_s).

SIMULATION IMPLEMENTATION

Based on the models of the previous sections, a digital computer simulation was developed on the Control Data Corporation 7600 machine. As shown in Figure 2, these models are grouped into an environmental block and a sensor block. The environmental block consists of a star field model, a zodiacal light model, an earth limb model, a resident space object model, and a nuclear radiation model. This block acts as a driver for the sensor block, which consists of an optics/scanner model, a focal plane detector model, an amplifier/filter model and a multiplexer/encoder model. In addition, provisions are made to include the effects of spacecraft attitude jitter, internal detector noise, and electronic noise.
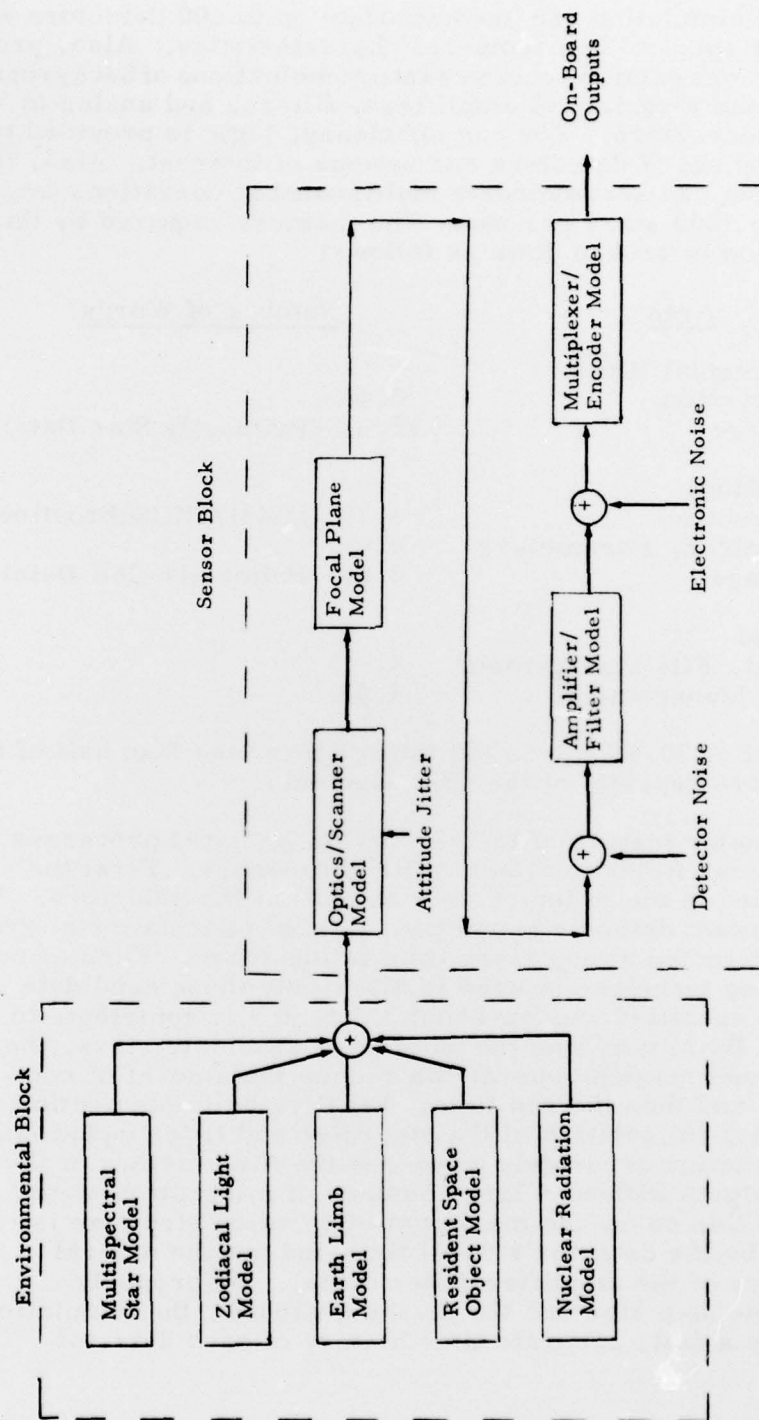
10

Figure 2. Block Diagram of a Scanning Sensor Simulation

11

The simulation can accommodate up to 100 detectors with different spectral and temperal characteristics. Also, program options exist to accommodate combinations of background models and a variety of amplifiers, filters, and analog to digital converters. For run efficiency, logic is provided to select the set of detectors and options of interest. Also, the simulation can accommodate multiscanning operations involving up to 3000 stars per run. The memory required by this simulation is broken down as follows:

Area	Number of Words
Environmental Block	
Instruction	0.4K
Storage	12.3K (Primarily Star Data)
Sensor Block	
Instruction	1.5K (Main)/1K (Subroutine)
Variables, Parameters	4.6K
Storage	2.6K (Primarily Cell Data)
Overhead	
Print, File Management	4.0K
Plot Management	4.0K

The total of 30.4K words (60 bit/word) is less than half of the small core capacity of the CDC Machine.

A major feature of the simulation is that it processes high density star fields in a fast, efficient manner. First the stars are sorted in the order of their arrival at the detectors. Then with a known detector geometry, a set of candidate stars that can be detected at any given time is identified. Furthermore, a masking technique is used to allow only those candidate stars within a specified window about a detector to contribute to its output. By minimizing the number of candidate stars, the sorting and masking operations reduce the amount of computation and thus the run time. Finally, by implementing a closed form solution of the amplifier and filter equations, the simulation accurately computes the time history of the filter outputs without a large number of integration steps/ run. In this case, the maximum integration step size is limited by the detector's dwell time and not the natural frequency of the amplifier/filter model. By properly sizing the step size and the masking window, the simulation provides a fast, accurate time history of each detector output.

Figure 3 shows the geometry of a typical run involving two linear arrays (5 detectors/array) scanning a celestial background consisting of stars, zodiacal light, and earth limb radiation. The run simulates a constant scan rate sensor, a band-pass filter providing A-C coupling, and a bipolar, analog-to-digital converter providing logarithmic compaction in the encoding process. Typical outputs of two adjacent detector channels are shown in Figures 4 and 5 for a field of view consisting of stars at a nominal density level and five times that level, respectively. The plots indicate the filter outputs, encoder outputs, and the outputs of a ground reconstruction filter that inverts the nonlinear encoding operation. It is noted that a high degree of fidelity exists between the on-board filter outputs and the reconstructed filter outputs.

The execution time for this simulation depends on the number of detector cells considered, the number of point sources scanned, and the number of integration steps/run. For example, the execution time was 8.3 seconds based on 10 detector cells, 100 stars, and 1254 integration steps/run. The execution time increased to 21 seconds when there were 500 stars in the field of view. For the same number of stars, the execution time is doubled when the length of the run is doubled. Thus the execution speed is more sensitive to the total number of integration steps than the total number of point sources scanned.

CONCLUSION

An approach for simulating scanning astronomical sensor systems has been presented. The approach is based on utilizing simple but reasonably accurate models of the sensor and its major radiation sources. Under reasonable assumptions, these models simplify the relations characterizing the signals and noise in the system. Based on these relations, a highly flexible digital simulation was developed. This simulation provides a tool for assessing on-board system performance and for testing ground data processing software.

The simulation utilizes sorting and masking techniques to reduce the amount of computations associated with high density sources. In addition, closed-form solutions of the differential equations were implemented to provide high fidelity results without a large number of integration steps per run. As a result, the simulation is capable of processing system outputs in a fast, efficient manner.
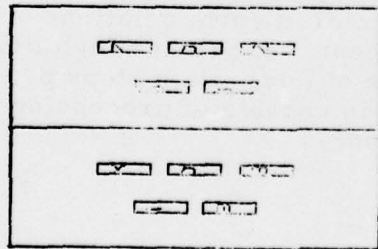
Star Field

Scan Direction

Cell Layout

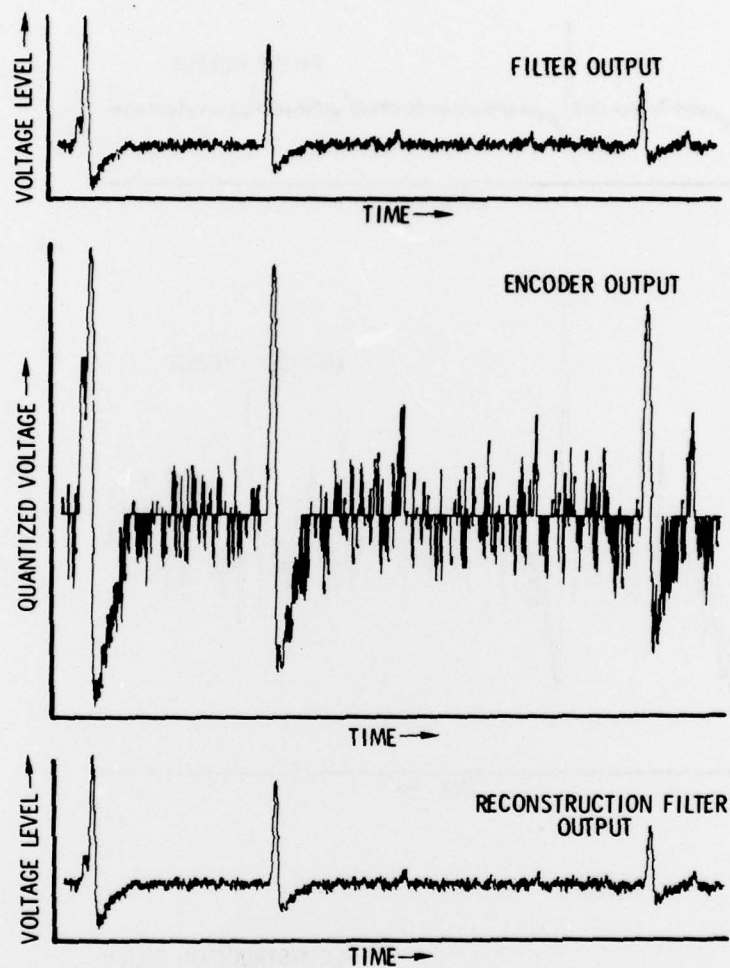Figure 3. Detector Cell Geometry for a Sample Run

Figure 4a.   Typical Outputs of Cell 1
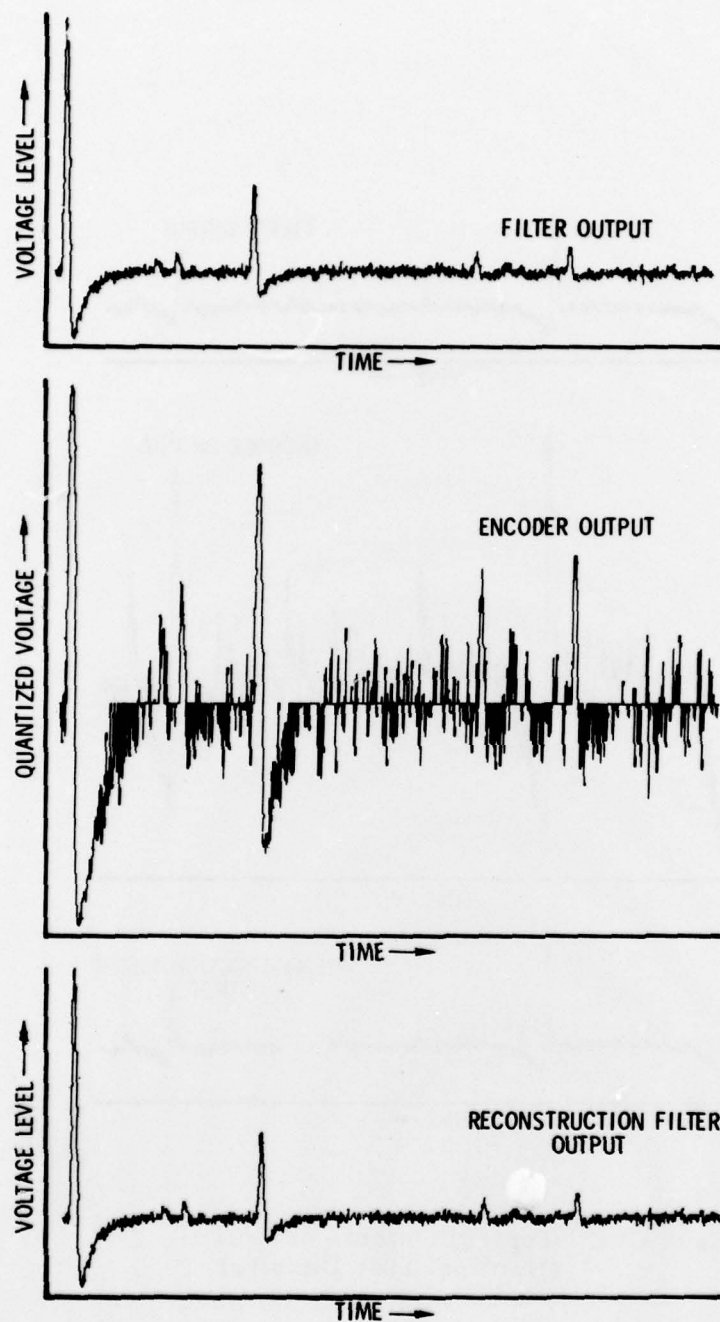(Nominal Star Density)

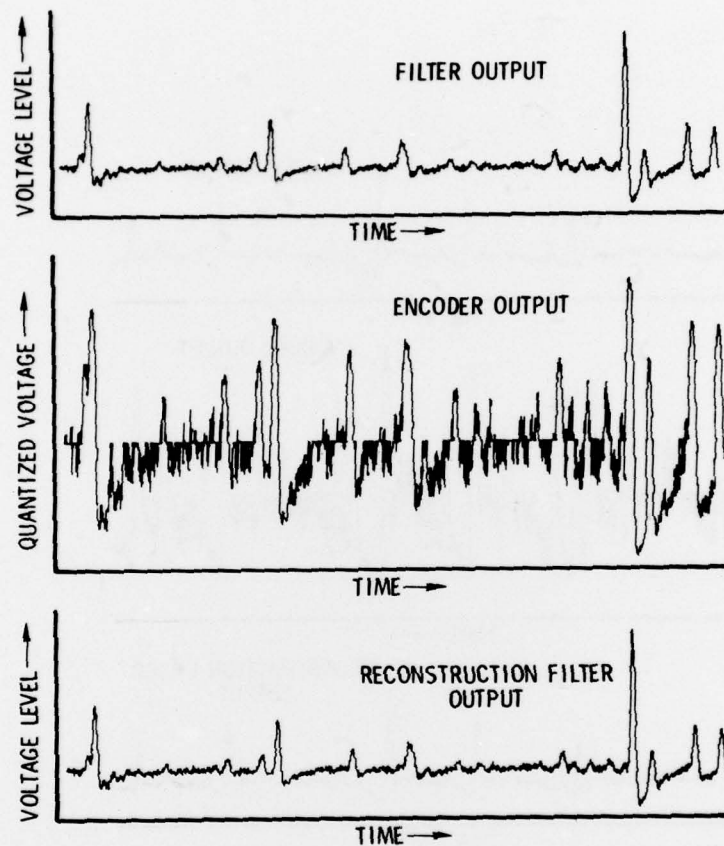Figure 4b. Typical Outputs of Cell 2
(Nominal Star Density)

16

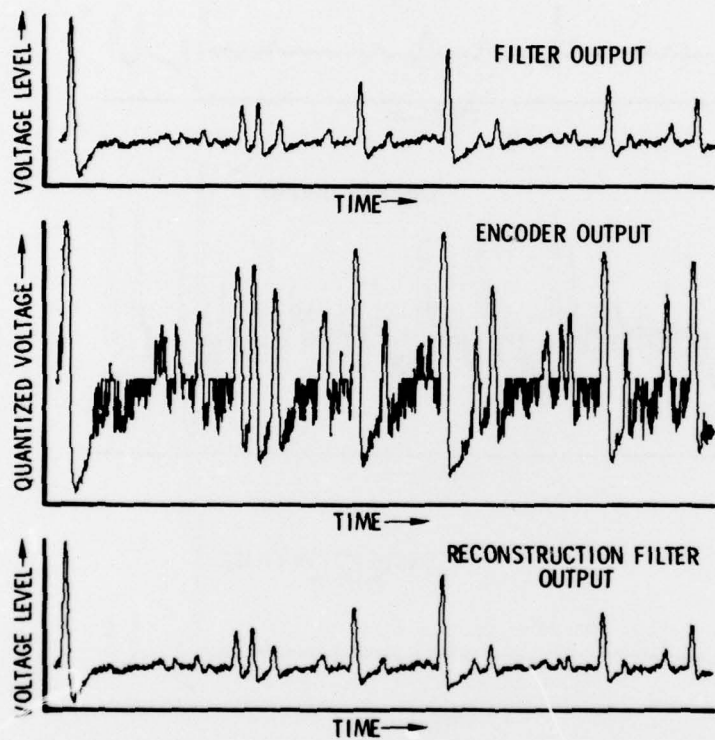Figure 5a.   Typical Outputs of Cell 1 (5X Nominal Star Density)

17

Figure 5b.   Typical Outputs of Cell 2 (5X Nominal Star Density)

REFERENCES

1. R. L. Hedden, "A Telescope for the Infrared Astronomical Satellite (IRAS)," Proceedings of the SPIE, Volume 95, pp 8-12, August 26-27, 1976.

2. E. M. Winter and M. C. Smith, "Processing Techniques for Infrared Astronomical Surveys," Proceedings of the SPIE, Volume 95, pp 147-155, August 25-26, 1977.

3. E. M. Winter and P. Stucki, "Techniques for the Simulation of Electro-Optical Sensor Systems," Proceedings of the 1977 SCSC, 1977, pp 865-870.

4. J. W. Cooley and J. W. Tukey, "An Algorithm for Machine Calculations of Complex Fourier Series," Mathematics of Computation, April, 1965.

5. E. M. Winter and D. P. Wisemiller, "Development of a Large-Scale Electro-Optical Simulation," Proceedings of the SPIE, pp 183-193, Volume 59, 1975.

6. D. Middleton, "On the Theory of Random Noise: Phenomenological Models I," Journal of Applied Physics, pp 1143-1152, Volume 22, 1951.

7. S. Karlin, A First Course in Stochastic Processes, Academic Press, New York, 1966, pp 183-184.